photochem

MDPI

Review

Plasmon-Induced Semiconductor-Based Photo-Thermal Catalysis: Fundamentals, Critical Aspects, Design, and Applications

Atif Sial, Afzal Ahmed Dar, Yifan Li and Chuanyi Wang *

School of Environmental Science and Engineering, Shaanxi University of Science and Technology, Xi'an 710021, China
* Correspondence: wangchuanyi@sust.edu.cn

Abstract: Photo-thermal catalysis is among the most effective alternative pathways used to perform chemical reactions under solar irradiation. The synergistic contributions of heat and light during photo-thermal catalytic processes can effectively improve reaction efficiency and alter design selectivity, even under operational instability. The present review focuses on the recent advances in photo-thermal-driven chemical reactions, basic physics behind the localized surface plasmon resonance (LSPR) formation and enhancement, pathways of charge carrier generation and transfer between plasmonic nanostructures and photo-thermal conversion, critical aspects influencing photo-thermal catalytic performance, tailored symmetry, and morphology engineering used to design efficient photo-thermal catalytic systems. By highlighting the multifield coupling benefits of plasmonic nanomaterials and semiconductor oxides, we summarized and discussed several recently developed photo-thermal catalysts and their catalytic performance in energy production (CO_2 conversion and H_2 dissociation), environmental protection (VOCs and dyes degradation), and organic compound synthesis (Olefins). Finally, the difficulties and future endeavors related to the design and engineering of photo-thermal catalysts were pointed out to draw the attention of researchers to this sustainable technology used for maximum solar energy utilization.

Keywords: photo-thermal catalysis; localized surface plasmon resonance; hot charge transfer pathways; photo-thermal conversion; morphology engineering

Citation: Sial, A.; Dar, A.A.; Li, Y.; Wang, C. Plasmon-Induced Semiconductor-Based Photo-Thermal Catalysis: Fundamentals, Critical Aspects, Design, and Applications. *Photochem* **2022**, *2*, 810–830. https://doi.org/10.3390/photochem2040052

Academic Editor: Isabella Natali Sora

Received: 14 September 2022
Accepted: 29 September 2022
Published: 2 October 2022

1. Introduction

At present, due to the intense rise in the overall population, accompanied with the massive industrial development and utilization of natural deposit, the world is cladding two critical problems: the preservation and aggravation of the environment and energy conservation, storage, and substitute transformation [1]. Several technologies have been applied on the laboratory and industrial scale to overcome the aforementioned challenges. Presently, material science and engineering is one of the trending research fields. The successful direction for a convincing practical application is to develop a material with distinctive and/or tailored properties [2]. Even though material engineering is the leading light behind the recent advances in technology, scientific societies keep using and improving material science to minimize the breach towards practical applications of smart materials in various fields covering the environment and energy disciplines [3].

Over the past few decades, the catalysis of chemical transformations via light as an energy source has become possible due to the discovery of heterogenous semiconductor-based photocatalytic techniques. The semiconductor generates an electron–hole pair after the absorption of a photon with equivalent or greater energy than its band gap. Ultimately, these generated hot charge carriers migrate towards the surface of the semiconductor and shift towards adsorbed molecules, thus initiating redox reactions [4]. After the innovative study of Fujishima and Honda in 1972, remarkable developments have been reported

in relation to the photocatalysis technique [5]. Still, the factor of low efficiency in most photocatalytic processes remains a bottleneck (usually within the range of hundreds of μmol g^{-1} h^{-1}), primarily because of the rapid recombination of charge carriers, the lower absorption rates, and the consumption of solar light energy through semiconductors with conventionally larger band gap [6].

Beyond hot charge carrier separation under light excitation, plasma-driven routes have been in the limelight. Excited charge carriers produced by the degeneration of localized surface plasmon resonance (LSPR) retains higher energy levels compared to the directly induced photoexcited charge carriers [7,8]. Moreover, these energetic carriers can also produce a thermal effect by internal relaxing and dissipating their energy levels through the local heat of the environs [9,10]. This generated heat has been extensively utilized in numerous fields, including cancer treatment, pollutant degradation, water splitting, and seawater desalination [11]. In a recent study, Nguyen et al. successfully synthesized a ternary heterostructure catalyst composed of TiN nanotubes, with TiO_2 as an intermediate layer connected with the $In_2O_{3-x}(OH)_y$ nanoparticles for CO_2 hydrogenation. The photocatalytic results of the study demonstrated that the three ordering components of the heterostructure proved to be beneficial for its activity in CO_2 photo-catalysis. Moreover, it was also stated that the TiN nanotubes not only induced the photo-thermal effect, but also provided a critical replacement to minimize the required amount of $In_2O_{3-x}(OH)_y$ nanoparticles, thus leading to an enhanced CO production rate, whereas the TiO_2 serves as an efficient charge transport path [12]. Photo-thermal catalysis, which syndicates heat- and light-based chemical influences, has appeared as a fast-developing and emerging novel research field [13]. Photo-thermal catalysis enables more efficient trapping of the solar energy in the light spectrum, covering visible and infrared photons which are otherwise inadequate to excite photocatalytic reactions [14,15]. In addition, during the photo-thermal catalytic process, the temperature of the catalytic sites rises; thereby, photo-thermal synergistic catalysis achieves exceptional production yields, even under normal operational conditions [16].

Due to the rapid expansion of the field, scientific communities from all around the world have been drawn to photo-thermal catalysis, which focuses on fuel generation and chemical production. As in recent years, special emphasis has been placed on the rudiments of the LSPR effect and the fundamental mechanisms underlying photocatalytic and thermocatalytic routes that delineate the basic concept of the photo-thermal catalytic process. Based on recent developments, novel characterization approaches and practices can help to determine the dominant reaction pathway for a certain catalytic system, thus facilitating a clear understanding. Afterward, for enhanced photo-thermal catalytic performance, collecting the most relevant knowledge available with regards to performance, target selection, and mechanistic insight is still needed. Following that, collecting the most appropriate information relevant to all the above-mentioned terms is still required for enhanced photo-thermal catalysis. Last but not least, the current focus is on designing techniques to further enhance catalytic efficiency and highlight the future applications and limitations. Therefore, this review summarizes the following: (i) fundamentals behind the photo-thermal effect and LSPR formation, (ii) mechanisms of charge carrier generation and the transfer from host to adsorbate, (iii) structural design and engineering of the catalysts for efficient photo-thermal catalysis, (iv) photo-thermal applications of catalytic systems in energy generation and conversion, chemical production, and environmental remediation, and (v) the potential drawbacks and future endeavors of photo-thermal catalytic systems.

2. Fundamentals of LSPR Formation in Photo-Thermal Catalysis

Plasmonic photocatalysts, as a heterostructure, have attracted significant attention due to their ubiquitous application in photocatalytic systems. There are three types of plasmonic catalyst heterostructures: the first type includes rare earth metals or noble metals (Au, Ag, Pd, etc.), which have been widely applied in the photo-thermal catalytic reactions due to their significant LSPR property and efficient light to heat conversion ability; the

second type mainly covers conducting oxides (RuO_2, metallic-doped oxides, etc.), which are considered as star materials in the field of the photocatalysis because of their wide range of light utilization in the whole solar spectrum; and the third type entails the transition of metal-based nanostructures, which are highly popular in the field of photo-thermal catalysis owing to their excellent performance in different catalytic reactions, such as CO_2 hydrogenation, Fischer–Tropsch synthesis (FTS), reverse water–gas shift (RWGS), and the dry reforming of methane (DRM) activity [7,9]. Similarly, these types have special characteristics and identification methods, as shown in Figure 1. In numerous metallic nanoparticles, localized surface plasmon resonance (LSPR) occurs when the wavelength of the photons ties the usual frequency of oscillating surface electrons in contrast to the restoring force of positive nuclei. It can be visualized as a coherent oscillation of conduction electrons [8]. An excited hot carrier is generated by dephasing the free-electron oscillation via a non-radiative energy dissipation pathway (also known as the Landau damping process) after the intra-band excitation of plasmonic nanoparticles (PNPs) (between the Fermi level and the sp conduction band) or the inter-band excitation of PNPs (between the d band and the sp conduction band) [10]. It is possible for hot carriers that are sufficiently energetic to inject electrons into the nearby surface adsorbates or semiconductors, causing surface chemical changes (at femtosecond to picosecond levels). In order to promote mass transfer and reaction rates, the exchange energy of hot carriers with phonon modes (at picosecond to nanosecond levels) can dissipate their energy into heat [13]. Based on the type of main driving force, plasmonic photocatalytic reactions tend to be conducted with plasmonic hot carriers, thus playing a major role in the reaction at ambient temperatures or at a low reaction temperatures (less than 100 °C), whereas photo-thermal heat plays an insignificant role [7]. Overall, the coupling of PNP-localized heating (hot carrier generation) with the semiconductor oxide carrier (light utilization by relaxation behaviors) induced the synergistic effect of photo-thermal catalysis; however, the heat generation in this process was caused by the photo-thermal conversion activity under light irradiation [15].

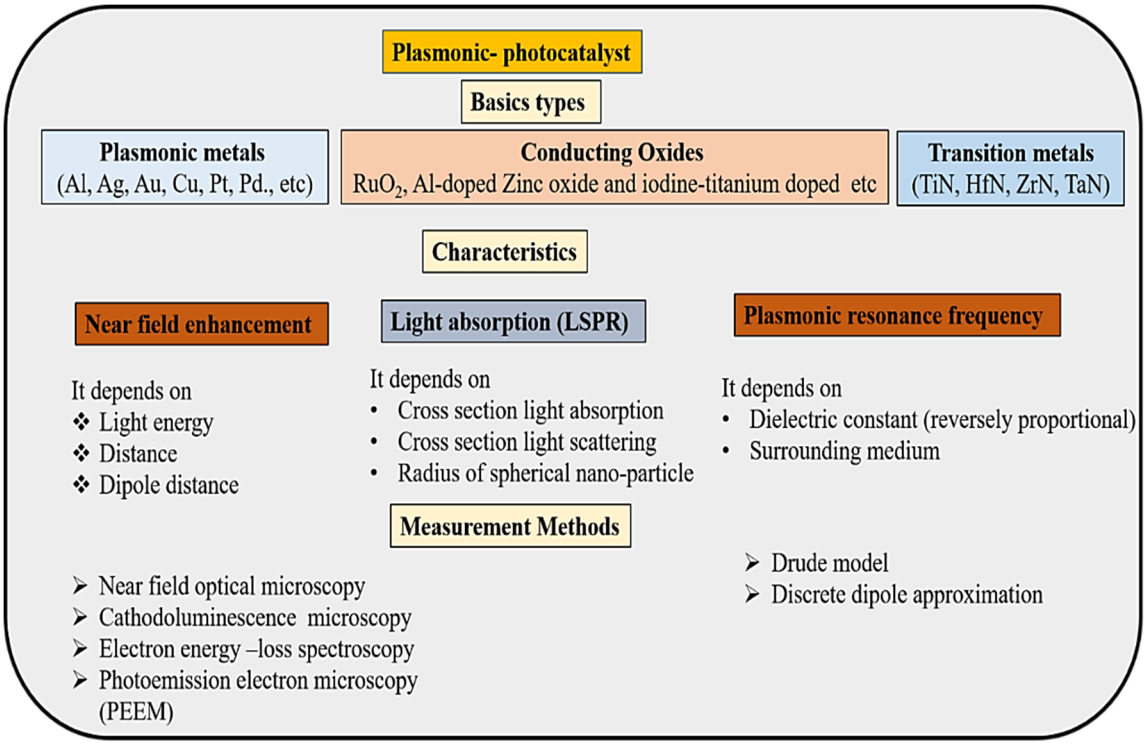

Figure 1. Basics of the plasmonic photocatalyst.

In plasmonic nanoparticles (PNPs), the localized surface plasmon resonance (LSPR) band is a strong and wide absorption band alongside the UV–visible NIR range of the electromagnetic spectra [13]. Plasmonic nanoparticles inducing the spherical-shape LSPR band is the most common and extensively applied theory in the plasmonic field. This signal is quelled by the inelastic motion of electron and the surface charge accumulation is generated after restoring the electron cloud (Figure 2). Generally, the LSPR band formed when the PNP size is smaller than the light wavelength. This phenomenon is explained by the quasi-static approximation process, in which the interaction between light and spherical PNP is directed by electrostatics instead of electrodynamics [17]. When compared to the primary cross-sectional absorption, the LSPR band enhances the light absorption rate by increasing the cross-sectional absorption to certain level [18,19].

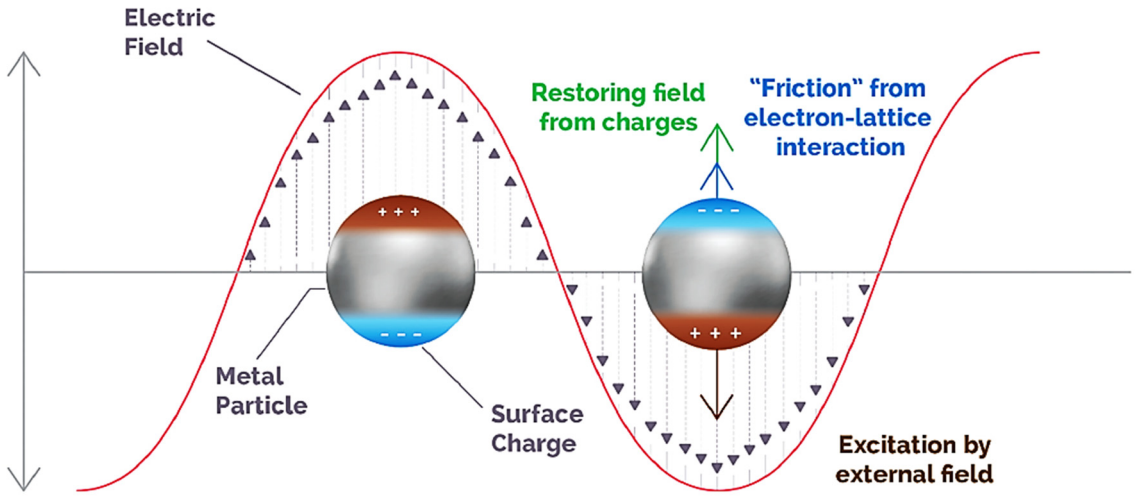

Figure 2. Schematic trends of a plasmonic nanoparticle under excitation. The (brown) color represents the incoming electromagnetic field and changes induced in it are followed by the motion of the carriers; thus, surface charges (blue) produce a restoring force towards the outer side of the equilibrium, and electron vibrational motions (blue) result in hindering caused by the ionic system. Reprinted with permission from Reference [20]. Copyright (2019) American Chemical Society.

Moreover, LSPR has the ability to generate a strong electric field around the external surface of the PNPs, which is even more powerful than the preliminary electric field of irradiated light [17]. This effect is known as near-field enhancement, and it is extremely beneficial for hot charge carrier generation process and transfer to nearby semiconductors [21].

Near-field enhancement, plasmonic resonance intensity, and LSPR effect-based light absorption are all important aspects of the LSPR that must be taken into consideration. The incident light and gap from the PNP outer surface have a significant impact on the near-field enhancement phenomenon [22]. Therefore, a light with a reliable intensity and a specific distance from the PNP surface is crucial to intensify the near-field enhancement.

3. Photo-Thermal Enhanced Catalysis

As stated previously, under plasmonic excitation, NPs generated hot charge carriers through the electronic transitions of intra-bands and/or inter-bands by non-radiative Landau damping [23]. The photons with energy *hn* speed up the excited electrons with energies greater the Fermi level (*EF* + *hn*), which can then be induced by the metallic nanoparticles to other species with electron-deficient orbitals. As a result of the plasmon-decaying process, the excited hot electrons shifted the kinetic energy towards the adsorbates, which are chemically stimulated by the transitions of electrical and vibrational motion [24]. Eventually, the higher-energy electrons shifted to the antibonding orbitals of interfacial species, creating a rift in the molecular bonds, and ultimately activating consequent chemical modifications.

These aforementioned hot charge carriers can be utilized in four major routes for different catalytic practices, depending on whether the plasmonic photocatalyst is a single-component or in a heterostructure form. The first two plasmon-based photocatalytic materials are associated with the use of hot charge carriers from sole plasmonic NPs that interact with adsorbates through direct or indirect transferring. In the other two routes, supported plasmonic nanostructures, which interacted with semiconductors via an indirect insertion pathway to carriers or acceptor species, are directly promoted into the conduction band (CB) [25,26].

3.1. Indirect Transfer of the Hot Electron into the Adsorbate

In the indirect transferring of electron, after plasmon activation, excited electrons are first generated in the metallic NP and then forwarded towards the lowest unoccupied molecular orbital (LUMO) of adsorbates on the metal surface [27,28]. As the electron shifting into the adsorbate occurs after the generation of hot charge carriers, it is thereby constrained by energy loss because of the scattering among electrons.

The performance of this indirect hot electron transfer route positively correlates with the incident energy of the photon, as higher energy generates more electrons with adequate potency to be inserted in the LUMO of adsorbates [29]. Such an indirect electron transfer route has been demonstrated in the plasmon-mediated excitation of different molecules, such as hydrogen (H_2) and oxygen (O_2) [30,31]. Lately, Halas et al., through DFT analysis and H/D exchange experimentations, confirmed that generated hot electrons on Au NPs could be transferred to the molecular H_2 antibonding orbital via an indirect transfer, resulting in negatively charged ${H_2}^{\delta-}$ species. Ultimately, electrons moved in a reverse direction towards Au and H_2, and then turned back to the ground state with aggregated vibrational energy, causing the eventual detachment of the H_2 molecule [32]. Linic et al. also successfully carried out the partial oxidation of ethylene with a plasmon-induced technique by employing Ag nanocubes. In the experiment, hot carriers were generated on the Ag nanocubes surface and indirectly transferred to O_2 antibonding sites, resulting to O_2 generation. Similar to the H_2 activation case, the aggregated vibrational energy incapacitated the limitation of activation energy and resulted in O_2 detachment [24]. Both the induced electromagnetic flux as well as the resonant frequency of excited carriers are used in the resonance phase; therefore, the maximum exploitation of the electric field in presumed vacancies takes place on the plasmonic NP surface. Additional LSPR-related properties rise from the different relaxation routes within plasmon-based structures, in addition to the larger electric field. After activation, the stored energy in surface plasmons can be degenerated in a variety of ways, either adopting irradiative (by re-emitting the photons) or non-irradiative pathways (by exciting the charge carriers and electron–electron collisions).

3.2. Direct Transfer of Hot Electron into the Adsorbate

The hot electrons can also be directly transferred from metal NPs into adsorbates via LSPR activation [33]. This plasmon phase-shifting process, developed by chemical interface damping (CID), occurred due to the interaction of vacant adsorbate states and activated surface plasmons [25]. In the direct transferring pathway, excited electrons are relocated straight into the hybridized states existed among the metallic nanoparticle and adsorbates [34]. As a result, unlike the indirect pathway, which occurs after the excitation of hot electron, direct transfer mechanism takes place concurrently during the phase-shifting of the plasmon activation [35]. Therefore, the direct pathway is estimated to have greater potential for electron transferring and lower energy deprivations because it avoids electron–electron scattering. Nonetheless, this possible route for direct electron excitation is less likely to occur, for the reason that it demands a strong interaction among adsorbate and metal for the hybridization of surface orbital, which is unusual in plasmonic photocatalysts [25].

Remarkably, Linic and co-workers' photo-degraded the methylene blue by using Ag nanocubes and observed that the hot electron was transferred through directly. The Ag nanocubes showed two absorption bands at the wavelength of 532 and 785 nm under

irradiation, and the maximum degradation efficiency was displayed at 785 nm. The results concluded that the extended wavelength retains lower energy, and thus can efficiently transfer hot electrons, suggesting the direct electron transfer instead of the indirect transfer pathway [28,34].

3.3. Indirect Transfer of Hot Electron into the Semiconductor

The methodology of supported plasmonic nanoparticles to absorb has been broadly explained in the photocatalysis field [36]. LSPR bands containing metallic NPs completely exploited solar light under visible and NIR regions. Moreover, the utilization of dual-plasmonic metal–semiconductor systems possesses the further benefit of supporting the spatial partition of photoexcited electron–hole pairs after hot electrons are transferred to the semiconductor, thus extending their lifetime by avoiding the recombination of charge carriers inside the metal [37,38].

The most convenient technique for excited electron transferring in heterostructures, similar to the indirect transfer method used for non-supported plasmonic NPs, includes hot electron generations in the plasmonic NP within the time frame of femtoseconds, thenceforth allowing the transfer of electrons via the interface of the metal–semiconductor hybrid system (Figure 3).

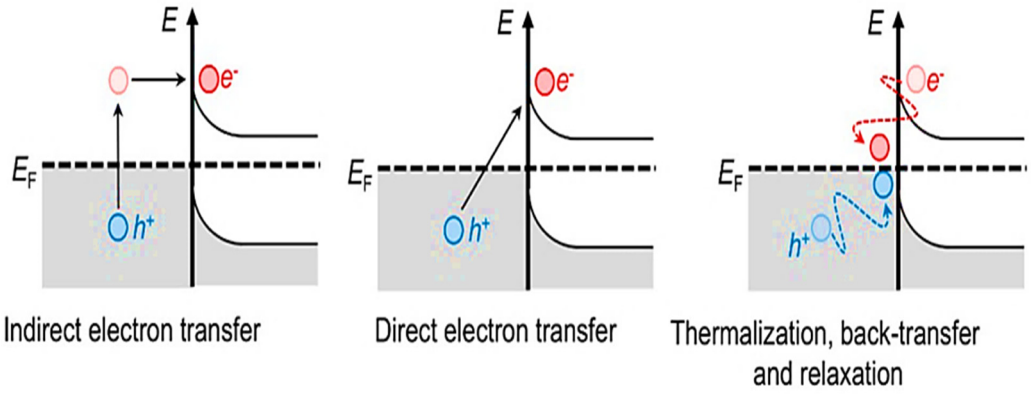

Figure 3. Schematic depictions of the hot charge carrier induced by plasmon and direct–indirect electron transfer processes along with the reverse motion in the metal–semiconductor heterosystem. Reprinted with permission from Reference [25]. Copyright (2017) American Chemical Society.

When a heterojunction is formed among the metal and semiconductor, the Fermi level of both participating species align to support the charge redistribution and system equilibrium (Figure 4) [39]. This effect tilters the valence and conduction bands of the semiconductor, resulting in the formation a Schottky barrier on the metal–semiconductor heterojunction interface whose energy (jSB) parallels to the difference in the metallic nanoparticle Fermi level and the edge of the CB interface [40].

Importantly, only photogenerated electrons with greater energy than the Schottky barrier energy threshold will be inserted into the CB and will be made accessible for further reactions induced by electrons at the semiconductor surface. Incidentally, the lower ϕ_{SB} promotes more charge carriers with higher energies to cross the barrier, and thus takes part in chemical transformations. Nonetheless, it is also critical that the bending at the interface of CB is sufficient to inhibit the back-flow of excited electrons towards the metallic nanoparticle, ensuring the spatial partition of charge carriers [20]. Therefore, while constructing heterojunction between metal and semiconductor, an appropriate equilibrium between these two effects must be considered.

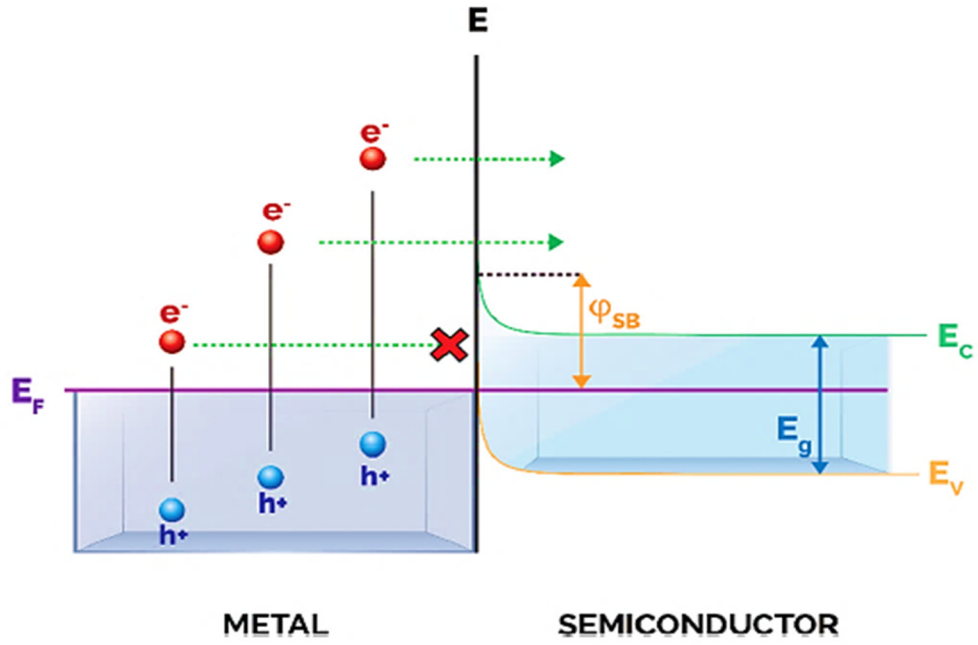

Figure 4. Schematic representation of Schottky barrier in the metal–semiconductor heterostructure. Upon irradiation, generated hot electrons with sufficient energy are able to pass through the Schottky barrier (ϕ_{SB}) junction and move to the CB of the semiconductor. Reprinted with permission from Reference [39]. Copyright (2014) Wiley-VCH.

Generally, the Schottky barrier scale lies in a range between 0.5 and 1.5 eV, and noticeably detects the insertion efficacy of the hot electron from the metal nanoparticle to the semiconductor conduction band [27]. Most importantly, the Schottky barrier length is shorter than the various semiconductors band gap, and this represents the major benefit of such heterostructures. As for their extraction, there is no need for the hot electrons to retain a higher energy level than the semiconductor band gap [41].

3.4. Direct Transfer of Hot Electron into the Semiconductor

Aside from the previous reported indirect hot electron transferring route, few other reports have mentioned the direct transfer pathway among metal–semiconductor heterojunctions (Figure 2). The timeframe for electron transfer in the indirect pathway is thought to be in picoseconds.

Furube et al. discovered a more rapid timescale for electron transfer in the range of hundreds of femtoseconds using transient absorption spectroscopy measurement results in Au/TiO_2 nanoparticles [42]. Furthermore, the actual quantum yield (QY) achieved in the transfer pathway was 40%, in contrast to the overall yield obtained during the indirect electron transferring mechanism, which was less than 8% [43]. In compliance with this research field, numerous studies have reported superfast hot electron insertion in the hybrid nanomaterials of a plasmonic metal–semiconductor, and some showed remarkably higher QYs [44,45]. The direct route is supposed to be more effective in transferring hot electrons from the plasmonic metal towards an adsorbate surface as it decreases the energy dissipation of hot electrons [46].

4. Influential Aspects Contributing to Photo-Thermal Catalysts

Photocatalysts should meet a number of characteristics in order to maximize the photo-thermal effect during the catalytic reaction, such as the intense absorption of light, the ability to generate more charge carriers, and the large capacity to produce and transfer heat [47]. A number of designing strategies are used to enhance the photo-thermal effects

and their efficiency in a certain mechanism. The two major factors responsible for the improved photo-thermal performance are as follows.

4.1. Effect of Size and Shape

To determine the LSPR phenomenon in the plasmonic materials, size and shape play a vital role and can be attuned properly, so that the plasmon band of the material could match with the solar spectrum and thus enhance catalytic activity [48]. In reality, both parameters exhibit a huge impact on the charge carrier generation and the thermal properties of the material.

Hypothetical analysis revealed that the plasmonic ability of nanoparticles is strongly dependent on the size, as large-size nanoparticles generate more charge carriers than small-size nanoparticles; however, their energy display is closer to the Fermi level [7]. In contrast, small-size nanoparticles have high energy levels but shorter lifetimes in the order of femtoseconds [49]. Therefore, small-size nanoparticles have great significance in photo-thermal catalytic reactions, due to the high energy level that they can overcome or cross the Schottky barriers, which seems to be more convenient for the hot electron-excited catalytic reaction. However, in the small-size nanoparticles based on photo-thermal reactions, due to the reduction in nanoparticle size, there are higher chances of the separation of charge carriers being inefficient [50]. Plasmonic nanoparticles, upon increasing the size, have also shown another distinctive feature of red shift in their resonance frequency, and thus can harvest the visible and IR regions of solar spectrum more efficiently [51].

Another major parameter of determining the optical properties of plasmonic nanostructures featuring the LSPR effect is morphology. Certain morphologies, such as nanobars and branched nanostructures, have shown the red-shift effect in their major LSPR absorption peaks, making them more appropriate for exploiting the lower-energy regions of the light spectrum [52]. Govorov et al. stated that the morphology of the plasmonic structures could also affect their hot carrier generation ability. In the experimental analysis, authors compared the defective and inhomogeneous geometries with the non-defected and uniform geometries. The final results concluded that the geometries with strong electric fields, when combined with the confinement effects, generated more hot electrons of higher energy levels, as compared to the non-defective or uniform electric field geometries, which produced lower-energy hot charge carriers [53,54].

The size and shape parameters can also be engineered by modifying phonon transport inductions in order to enhance the thermal properties of the plasmonic nanomaterials. For example, the thermal conduction properties of the plasmonic material were reduced in some reports by applying high-density grain barriers, which then amplifies the phonon scattering process [46]. Similarly, increasing the surface roughness can also decrease the phonon speed [55]. Therefore, an adequate balance between all above-described factors should be carefully examined when designing and engineering photo-thermal catalysts.

4.2. Designing the Hybrid-Structure System

The design of hybrid materials is another alternative and frequently applied technique used to enhance photo-thermal activity. In this strategy, composite structures sharing different light, heat, and electrical properties improve photocatalytic performance by generating synergism. In general, photo-thermal heterojunctions consist of an inorganic host (mostly metallic oxides facilitated by plasmonic or non-plasmonic metal NPs). It is also noteworthy that every component is not limited to play a single role within the photo-thermal heterojunction, and either one or more elements can serve as an active site in the catalytic reaction due to the nature of each composite material [46].

4.2.1. Metal–Semiconductor Hybrid Systems

As mentioned above, hybrid structures consisting of metals and semiconductors are extensively studied in photo-thermal catalytic reactions. An ideal semiconductor should display extraordinary characteristics, such as a large surface area and a wide range of light

absorption, to generate hot charge carriers. In that case, metal oxide semiconductors are the most feasible materials, showing a higher degree of defects along with mid-band gap states that eventually intensify the optical absorption in the lower-energy regions of the light spectrum [56]. In another study, Ozin et al. tested the photo-thermal effect based on CO_2 hydrogenation by using an unknown chemical ratio of black In_2O_{3-x}/In_2O_3 nanomaterial [57]. The findings revealed that the hydroxylation of pale yellow In_2O_3 at various temperatures produced non-stoichiometric black heterostructures made up of In_2O_{3-x} domains in single-crystal stoichiometric In_2O_3. These heterostructures showed wide-range absorption across the light spectrum, resulting in outstanding photo-thermal activity. The photo-excitation generated a strong thermal response within the In_2O_{3-x}/In_2O_3 nanostructures, also because the mid-gap states associated with photo-induced electrons enhanced the photochemical hydrogenation of CO_2. The utilization of semiconductors in such a wide light absorption range, either alone or in combined form with certain metallic active sites, can provide new directions in the design of efficient photo-thermal systems.

4.2.2. Metal–Porous Hybrid Systems

MOFs and zeolites, which have high porosity and larger surface area, have been extensively used as hosts or supporting materials for metallic nanoparticles in a wide range of catalytic approaches. On the other hand, very little knowledge is available on these types of materials in the field of photo-thermal catalytic reactions.

In a recent study, Maspoch and co-researchers investigated the photo-thermal catalytic response of a range of MOFs by covering the main subdivisions of such kind of porous structure and evaluated the photo-thermal efficiency of each MOF [49]. In the experiment, the temperatures of UiO-66-NH_2 and CPO-27-Ni reached up to 149 °C and 167 °C, respectively, after half an hour of light irradiation, and the photo-thermal rates obtained for both composites were higher than 55%. Conversely, under similar operational parameters, the temperatures of UiO-66 and ZIF-8 composites raised to 57 °C and 70 °C, respectively, and the resulting photo-thermal rates were even smaller than 10%. The above results showed that the obtained photo-thermal efficiency was strongly reliant on the MOF light absorption band.

Although a lot is yet to be discovered, few other porous nanostructures, such as zeolites, have also been reported as active components in photo-thermal catalytic processes. Zhu et al. determined the photocatalytic response rate by oxidizing the benzyl alcohol and derivatives under visible-light irradiation [58]. The author immobilized the Au nanoparticles on the zeolite surface. According to the proposed reaction mechanism of the study, zeolite support in the composite system efficiently adsorbed alcoholic compounds, while Au nanoparticles played the role in O_2 activation by transferring plasmon-excited hot carriers. The kinetic study results also confirmed that the plasmonic effect reduced the excitation barrier by 40%.

4.2.3. Core–Shell Hybrid Systems

Due to the bifunctional ability, core–shell hybrid systems offer the benefits of tunable light, heat, and electrical properties, and illustrate a very appealing designing technique for new nanomaterials with excellent photo-thermal activity [59].

For instance, Yang and co-workers designed AuCu-CuS core–shell hybrid nanostructures stabilized on a TiO_2 surface [60]. The resulting synergic contribution of photo-thermal local heat and LSPR increased the photocatalytic oxidation of glycerol. Generated hot-electrons were abundantly transferred from the AuCu nanoalloy to the CB of TiO_2, and reacted with molecular O_2 to yield either H_2O_2 or reactive superoxide species (O^{2-}) which derived the glycerol oxidation. In the meantime, the thermal heating effect in the plasmonic CuS shell, due to the non-irradiative electron–hole pair recombination, further contributed in the entire catalytic reaction.

Xiong et al. successfully fine-tuned the shell thickness of the Pd in the Au nanorods to design a core–shell nanocomposite system for the styrene hydrogenation [61]. The author

stated that during photo-thermal catalysis, the core–shell hybrid system controlled both the local heating effect as well as the hot electron transferring pathway.

5. Photo-Thermal Effect-Based Applications

5.1. Solar Fuel Generation

The urgent need of green energy motivates the researchers to discover new energy materials and conversion technologies. Solar-light-based fuel production involves the utilization of solar energy to initiate chemical reactions and generates low-cost energy. Generally, plasmon thermal photocatalysis mainly yields certain types of chemicals and fuels, including methane and CO, which are reliant on the number of excited electrons. Over the past decade, to expedite the above-mentioned methods, the usage of photothermal-based catalysis has risen substantially. Few major applications of photo-thermal catalysts associated with the synthesis of fuels, organic compounds, and pollutant degradation are enlisted (in Table 1) and discussed further in the following section.

Table 1. List of several photocatalysts applied in photo-thermal catalysis.

Photocatalysts	Plasmonic NPs	Light Source	Absorption Wavelength (nm)	Temperature (°C)	Application	Ref.
Au-Pd nanostructures	Au nanorods	1.68 W Laser, 809 nm	ca. 809	62	Suzuki coupling reactions	[62]
Pd/WO_{3-x}	WO_{3-x}	Xe lamp	400–1100	60	Suzuki coupling reactions	[63]
Ag-TiO_2	Ag	150 W Xe lamp	200–1200	-	4-NP reduction	[64]
LaB_6@SiO_2/Au	LaB_6	CW 808 nm diode laser, 808 nm, 2.7 W m^{-2}	400–1200	40.5	4-NP reduction	[65]
Aue-ZnO	Au	Laser, 532 nm, 8×10^5 Wm^{-2}	ca. 538	600	CO_2 reduction	[66]
Group VIII metals/Al_2O_3	Group VIII metal	300 W Xe lamp	300–2500	300–400	CO_2 reduction	[67]
Ru@FL-LDHs	Ru	300 W Xe lamp	250–1500	350	CO_2 reduction	[68]
Fe@C	Fe	300 W Xe lamp	300–2500	481	CO_2 reduction	[69]
Al@Cu_2O	Al	10 Wcm^{-2}, VIS-light	300–1000	175	CO_2 reduction	[70]
Pd@Nb_2O_5	Pd	300 W Xe lamp, 18 kW m^{-2}	250–2400	200	CO_2 reduction	[15]
Ru/SiNW	SiNW	Xe lamp	300–2500	125	CO_2 reduction	[14]
Cu_7S_4@ZIF-8	Cu_7S_4	Xe lamp, 700 mW cm^{-2}	250–2500	122	Cyclocondensation reaction	[71]
Flower-like CuS	CuS	Xe lamp, 10 kW m^{-2}	300–900	65	Methylene blue degradation	[72]
Pd NCs@ZIF-8	Pd Ncs	Xe lamp, 100 mW cm^{-2}	220–700	34	Hydrogenation reactions	[73]
Cu-RM-C	MnO_2	Xe lamp, 96.3 mW m^{-2}	200–2400	120	VOC oxidation	[74]
SS-Co_3O_4	Co_3O_4	Xe lamp, 500 mWcm^{-2}	200–1500	175	VOC oxidation	[75]
Au@TiO_2 yolk shell	Au	300 W Xe lamp	-	-	Methane production	[76]
Ag-TiO_2 hollow-sphere	Ag	300 W Xe lamp ($\lambda > 420$ nm)	-	-	Methane production	[77]
Ag@LixTiO_2 nanocubes	Ag	Xe lamp 100 mW/cm^2 ($\lambda = 420$ nm)	-	-	Methane production	[78]
Ag-MgO-TiO_2 nanofibrous	Ag	300 W Xe lamp	-	-	Methane production	[79]
Au-Cu alloys/TiO_2	Au-Cu	1000 W Xe lamp AM 1.5 filter	-	-	Methane production	[80]
Pd-ZnO nanosheets	Pd	300 W Xe lamp	-	-	Methane production	[81]
Ni-modified Ni-Gehydroxide	Ni	300 W Xe lamp	-	-	CO generation	[82]
Au NR@ZnO	Au	300 W Xe lamp	-	-	CO generation	[83]
Ag-ZnO nanosheets	Ag	300 W Xe lamp	-	-	CO generation	[81]
Al@Cu_2O antenna heterostructures	Al	Supercontinuum fiber laser ($400 < \lambda < 850$ nm)	-	-	CO generation	[70]
P25-rGO	rGO	Xe lamp	250–800	36	MB reduction	[84]
Pt/PCN-224(Zn)	PCN-224(Zn)	Xe lamp	300–800	36	Benzyl alcohol oxidation	[85]
Pt@TiO_2-Au nanodendrites	Au	Xe lamp, 5.71 Wcm^{-2}	-	-	Methyl alcohol production	[86]

5.2. CO_2 Reduction

The production of fuels and chemicals through the water and CO_2 reaction is one of the most promising technologies used to neutralize the CO_2 in order to use in the transportation and chemical industry. At the present time, CO_2 reduction was mainly accomplished by the photocatalysis or two-step thermochemical redox reactions of metallic oxides (Zn/ZnO, Ce_2O_3/CeO_2, FeO/Fe_3O_4 and SnO/SnO_2) [87]; however, both reduction techniques have challenges of lower yield and a high-temperature requirements of around 2000 °C during the operation process. In contrast, the photo-thermal base CO_2 reduction appears to be an effective and simple route to reduce CO_2 at moderate conditions.

Various groups have investigated CO_2 reduction by photo-driven thermocatalysis. Ye et al. sustained the temperature between 300 and 400 °C by applying group VIII nano-catalysts and obtained photo-thermal CO_2 reaction efficiency (mol h^{-1} g^{-1}) with a

larger magnitude than those observed by simple photocatalysis (μmol h^{-1} g^{-1}) [87]. There was no significant variance among the CH_4 production by thermocatalysis and photo-thermocatalysis (Figure 4), and the CH_4 production rate was negligible under non-thermal irradiation with simple monochromatic light, implying that the reaction was performed by photo-driven thermocatalysis. Their later study of CO_2 evolution was also investigated on Ru@FL-LDHs by photo-driven thermocatalysis [68]. The obtained CH_4 evolution rate (277 mmol h^{-1} g^{-1}), which was parallel to that of thermocatalysis, was greater than all of the previously reported studies on LDH-based catalysts and other nanomaterials. Thus, the influence of photocatalysis can be neglected. In another study reported by Chen et al., where a CoFe alloy supported by alumina was synthesized to determine catalytic performance, the results showed nearly similar catalytic performance for the CoFe-650 catalyst under UV–vis light excitation, and was directly heated from outside at the same temperature (Figure 5b) [88].

A CO_2 reduction through the photo-thermal co-catalytic reaction has also been reported. Zhao et al. successfully produced CH_4 by using m-WO_{3-x} under photo-thermal conditions. The obtained value (25.77 μmol g^{-1}) after 12 h of irradiation was much higher than the values under thermal (21.42 μmol g^{-1}) and vis-light illumination (0.15 μmol g^{-1}) conditions. Therefore, an exclusive synergistic photo-thermal catalytic effect is generated via the meantime insertion of both catalytic systems [89]. The same group also determined the CH_4 evolution efficiency by using DOM-LSCF as a photocatalyst, and stated that the optimal performance of the photocatalyst was five times greater under photo-thermal conditions than that of sole thermal treatment conditions [90].

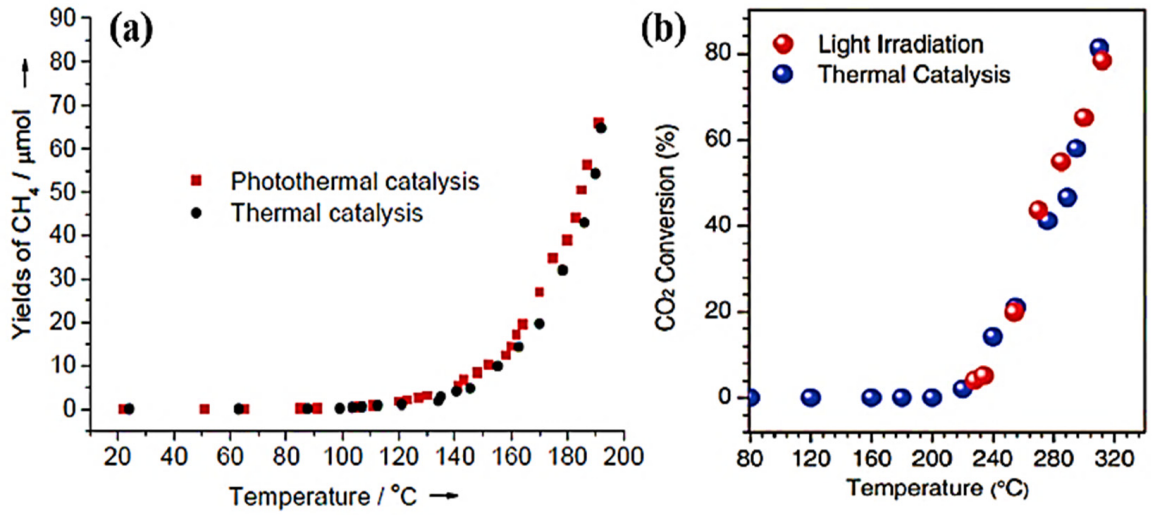

Figure 5. (**a**) CH_4 production by Ru/Al_2O_3 photocatalyst under combined photo-thermal and sole thermocatalytic conditions, under both treatments, where temperature was fixed by light source (300 W Xe lamp) and the whole reaction was carried out in the CO_2 and H_2 gas mixture. Then, 0.1 g of sample was taken and spread onto a spherical shaped filter. (**b**) CO_2 evaluation of CoFe-650 photocatalyst during photo-thermal irradiation (with UV–vis light) and direct heating without any light irradiation. Adopted with permission from Reference [91]. Copyright (2020) Elsevier Ltd. All rights reserved.

5.3. H_2 Evolution

Solar-light-based water splitting is a promising alternative for the H_2 evolution and is achieved by various electrolysis and catalysis techniques. Among them, photocatalysis has been proven to be the easiest and most direct pathway in which solar light is directly employed to split water into H_2 gas. However, it has certain limitations, such as a slow reaction rate, along with poor solar light absorption and conversion efficiency. In contrast, thermo-assisted photocatalysis has been demonstrated as the simplest pathway for direct

photocatalytic H_2 evolution. Ho et al. measured the H_2 evolution rate by fabricating the CuO on the TiO_2 surface. Results demonstrated that the photocatalyst exhibited 40 times higher H_2 evolution yield during photocatalysis by increasing the reaction temperature from 25 to 90 °C [92]. Furthermore, they also determined the photo-thermal performance of SiO_2/Ag@TiO_2 in seawater catalysis [93]. According the authors, the catalytic property of the photocatalyst was increased with an increase in temperature for altered sacrificial chemical components (Figure 6). Among all sacrificial reagents, glycerol achieved the maximum H_2 generation rate of 56.6% when the temperature increased from 30 to 90 °C. Likewise, Liu et al. acquired the H_2 evolution amount (27.4 mmol g^{-1}) with the Pt/TiO_2 photocatalyst under UV–vis IR light, which was twice the value (13 mmol g^{-1}) obtained under UV–vis irradiation [94].

In addition, Kubacka et al. reported the photo-thermal production of H_2 in a gas phase using methanol as a sacrificial agent by fabricating a noble metal ruthenium-doped catalyst (Ru/TiO_2) in a different weight ratio from 1 to 10 wt%. The photo-thermal catalytic performance was more significant than thermal catalysis within the temperature range of 120 to 300 °C. The authors also demonstrated that a clear synergy among light and heat was observed with temperatures up to 240 °C and then decreased subsequently [95]. In another report, Zhang and co-workers hydrothermally synthesized the (Ni/RGO) catalyst and applied the hydrogen evolution reaction by combining the photo-thermal and electrocatalysis processes. The catalytic activity of the prepared catalytic system was compared under light irradiation and in dark conditions, and the comparison results clearly demonstrated that light enhanced both the kinetics and the thermodynamics of the reaction, yielding superior H_2 evolution activity. The researchers described this unique etiquette with the capacity of the irradiated photocatalyst to generate excited carriers after absorbing the light; therefore, the temperature of the system was increased to 50 °C wit in 5 min [96]. Thus, operational temperature and optimum light irradiation both play a key role in the efficiency of the certain photo-thermal catalytic system and develop an adjustable synergism between light and thermal effect.

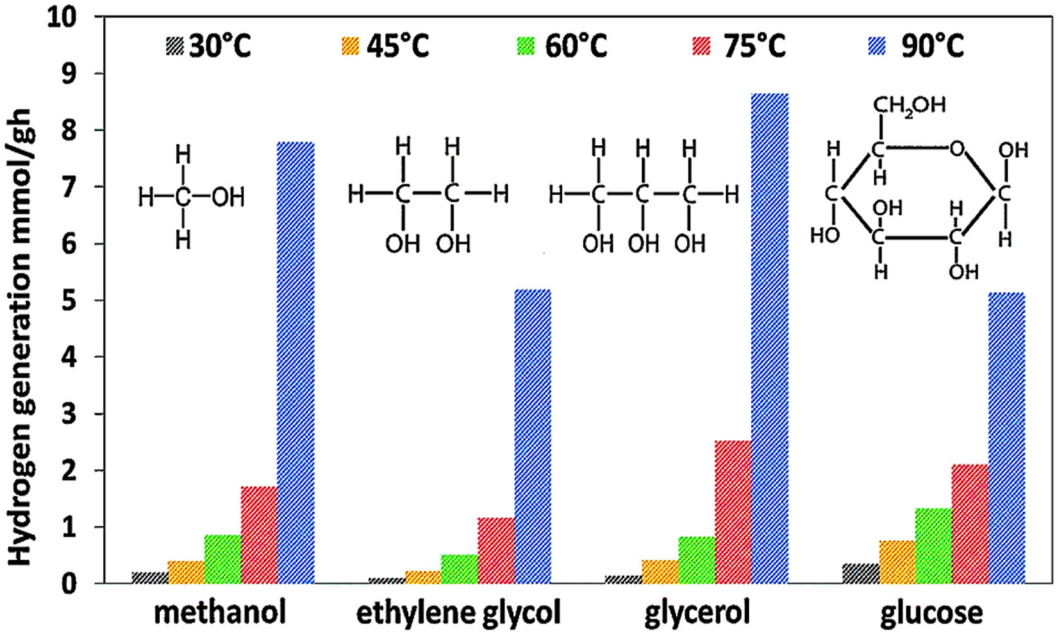

Figure 6. H_2 production of TiO_2 spheres in the solution of methanol (10% v/v), ethylene glycol (25% v/v), glycerol (20% v/v), and glucose (0.5 g) at variant temperatures. Adapted with permission from Reference [93]. Copyright (2016) Royal Society of Chemistry.

5.4. Organic Compound Degradation and Production

It is highly desirable to develop sustainable technologies to degrade various types of organic pollutants in air and water, such as volatile organic compounds (VOCs), 4-NP, and methylene blue (MB). The photo-thermal catalytic process seems a practical approach in environmental remediation as it utilizes both the light and heat energy of the solar spectrum.

Numerous studies have reported on VOC abatement, including acetone, benzene, and toluene, which are crucial air-polluting agents and cause damage to humans as well as the atmosphere. Photo-thermal catalysis has gained serious attention in this field because it can utilize the whole light spectrum covering UV, VIS, and NIR ranges. In this aspect, Li et al. reported the photo-thermocatalytic oxidation of benzene by coating the TiO_2 on a Hg lamp without any additional heat and light source. The obtained photo-thermocatalytic rate constant (K_{PTC}) was 2.4 times greater than the total sum of K_{PC} and K_{TC} [97], suggesting the synergistic use of UV light and heat from the Hg lamp, therefore belonging to the photo-thermal co-catalytic reaction. The similar co-catalytic effect of heat and light was observed in a study reported by [98], in which quite a different type of photo-thermal synergic effect was observed. In the experiment, the Hg lamp coated by the ZnO powder was used for the gaseous phase photo-thermal catalytic oxidation of acetone. Almost no CO_2 production was observed at 240 °C without UV-light irradiation. In contrast, the photocatalytic activity of the ZnO powder was increased with the temperature increase from 40 °C to 240 °C, and the amount of CO_2 production increased from 10.7 to 173.1 mg m^{-3}, respectively.

Dyes are one of the most common organic pollutants present in waste effluents from different industries, and are thus considered a bottleneck in wastewater purification technologies due to their larger volume, high toxicity, and slow biodegradation rate. In this scenario, the photo-thermal catalytic reaction has proven to be an effective technique due to its lower cost, operational sustainability, and renewable solar energy consumption.

There has been extensive interest surrounding the construction of efficient catalysts to convert the toxic 4-NP into the non-toxic 4-AP. In various reports on the photo-thermal catalytic-based reduction of 4-NP, the catalytic reaction in the existence of $NaBH_4$ can take place without any light exposure, and has been proven to be temperature-dependent. Therefore, the photo-thermally improved performance can be attributed to photo-assisted thermocatalysis. Kim et al. successfully suspended the Au nanoparticles on a filter paper and examined the photo-thermocatalytic activity in the 4-NP reduction [99]. The 4-NP was reduced more rapidly with the light irradiation than under dark conditions due to the photo-thermal activity of Au nanoparticles. It was also noticed that the reduction rate was marginally higher under light-irradiated processes than under dark conditions at the same temperature (Figure 7).

Photo-thermal synergic interaction mode is also applied to degrade certain dyes, in which thermocatalysis shows no activity, but the photocatalytic activity of the catalytic system is increased with the increase in reaction temperature. Wang et al. degraded the methylene blue (MB) via thermal-assisted photocatalysis by constructing the $Mn_3O_4/MnCO_3$ system [100]. The system showed negligible degradation under the dark or irradiation at 20 °C, while under visible-light exposure, the degradation rate was increased with increasing of temperature (Figure 8a). Consequently, the enhanced catalytic performance of the $Mn_3O_4/MnCO_3$ nanocomposite under photo-thermal effects was not only because of the photocatalysis and thermocatalysis, but also due the existence of synergistic influence which existed in $Mn_3O_4/MnCO_3$ nanocomposites, infatuating significant oxygen present in the lattice to entrap the holes, which then led to efficient oxidization at high temperatures (Figure 8b). Huang et al. synthesized the nanocomposite system of cerium oxide–cerium nitride (CeO_2/CeN) to degrade MB in wastewater using the photo-thermal catalytic method. No degradation efficiency was obtained after heating the solution to 80 °C under dark, while the photocatalyst showed a 90% degradation rate in 1 h below 25 °C, and obtained a 100% degradation rate in 30 min without the temperature regulation, signi-

fying that the thermal effect generated by light irradiation enhanced the photodegradation efficiency [101].

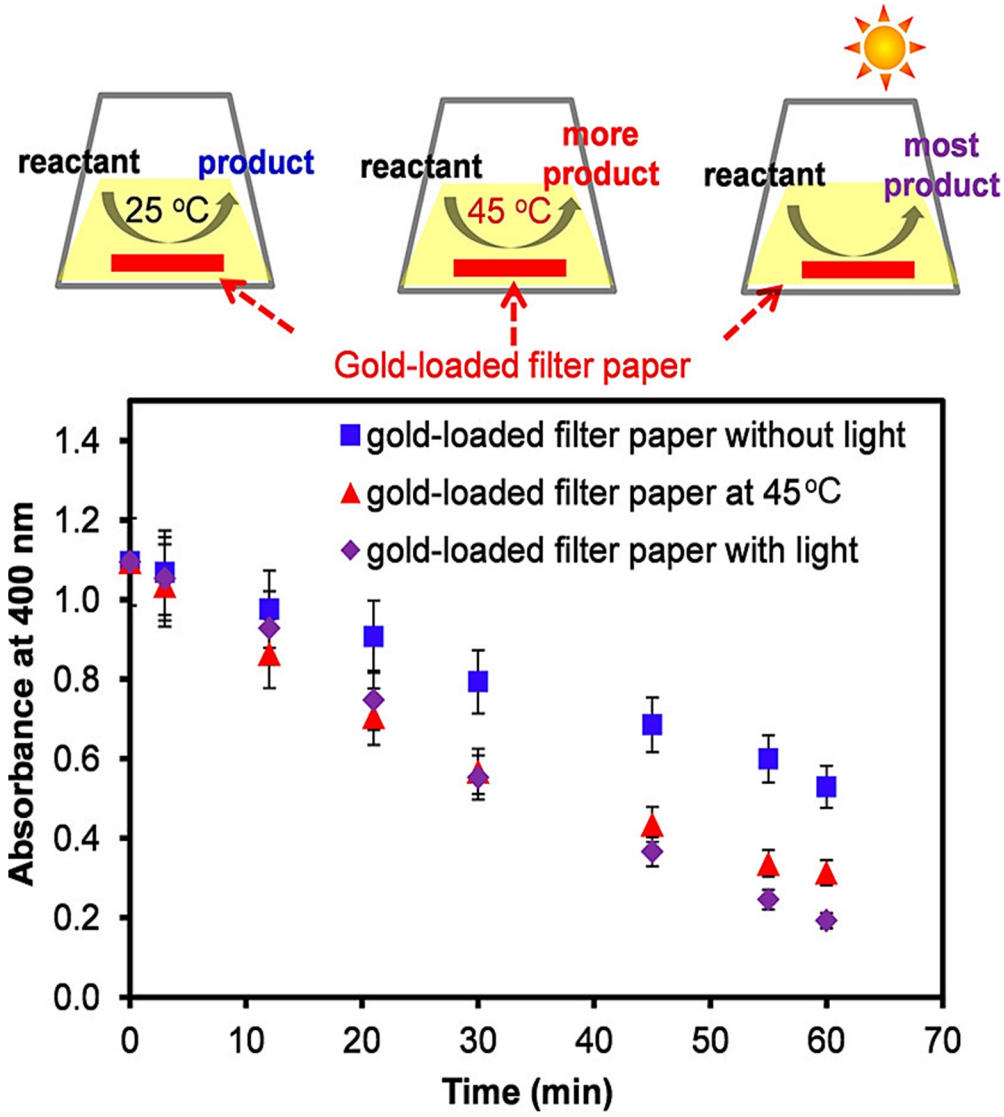

Figure 7. Absorption trends of 4-NP overloaded with the gold NP-coated filter paper without light (blue) and with the solar light irradiation (purple) and the gold-loaded NPs solution heated at 45 °C (red). The absorbance rate of 4-NP significantly decreased at the 400 nm intensity and a new absorption peak emerged at 300 nm, representing the 4-AP formation. Adapted with permission from Reference [99]. Copyright (2014) Royal Society of Chemistry.

Besides energy production and environmental protection, the photo-thermal catalytic method has also been utilized in the synthesis of organic compounds. An organic reaction is strongly correlated with a heat-derived catalytic process and intensely affected by temperature of the reaction, thus making it quite relevant to photo-thermocatalysis [102]. Christopher et al. derived ethylene epoxidation by depositing Ag nanocubes on the Al_2O_3 surface [24]. The results demonstrated that under an irradiation at 430 K, the steady-state ethylene epoxidation rate was four times greater than the rate of pure thermocatalysis.

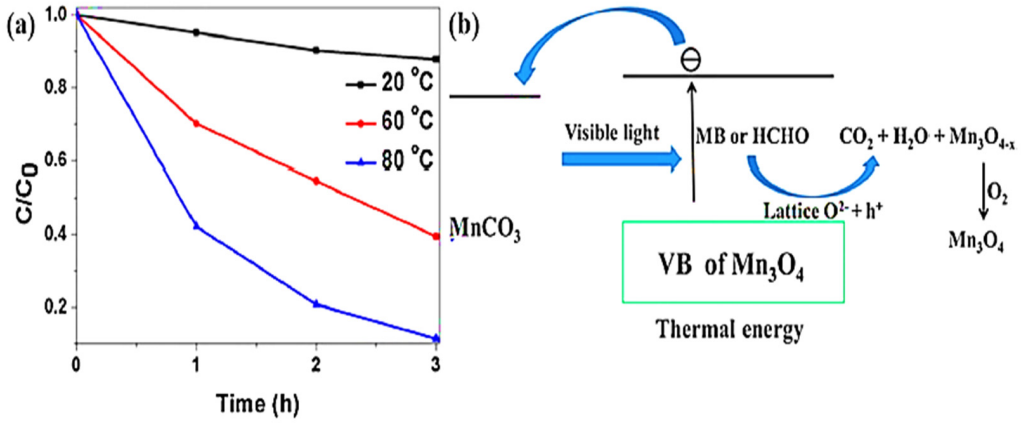

Figure 8. (**a**) Irradiation and thermal route of MB degradation at variant temperatures (20, 60, and 80 °C). (**b**) The proposed interaction mechanism of the coupled light and heat effect. Adapted with permission from Reference [101]. Copyright (2020) Elsevier Ltd. All rights reserved.

In another example, Wang et al. performed a cyclic condensation reaction by applying Cu_7S_4@ZIF-8 nanocomposites (Figure 9a) [103]. Figure 9b shows that the conversion rate of the photo-thermal catalytic process reached 97.2% within 6 h of irradiation, while at temperatures of 43 °C and 20 °C, pure thermocatalysis rates were only up to 55.4% and 18.1%, correspondingly. The conversion rate of 93.5% was finally reached at 43 °C by extending the reaction duration to 18 h, indicating that the traditional heating process was very time-consuming. Figure 9c demonstrates that the local heating-enhanced reaction efficiency was more than double that obtained by overall heating.

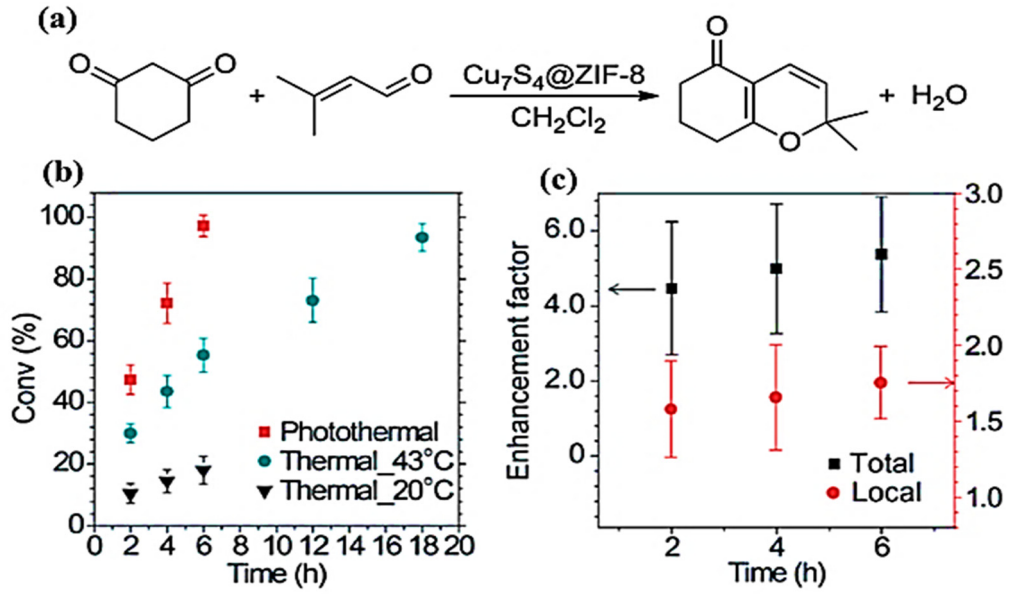

Figure 9. (**a**) Model photo-thermocatalysis of Cu_7S_4@ZIF-8 nanocomposites in the cyclocondensation reaction process. (**b**) Transformation rate of the cyclocondensation reaction process by photo-thermocatalysis and thermalcatalysis as a function of the reaction time. The photo-thermocatalytic reaction was regulated under laser light irradiation (1450 nm, 500 mW cm^{-2}) with no thermostatic regulation and the bulk reaction solution reached a maximum temperature of 43.3 °C. (**c**) Overall and amplification factor of localized conversion was determined by dividing the photo-thermally converted efficiency by the thermally converted efficiency at 20 °C and 43 °C, correspondingly. Reprinted with permission from Reference [103]. Copyright (2016) Royal Society of Chemistry.

6. Conclusions and Perspective

In recent years, plasmonic photocatalysts have attracted huge attention in relation to the photo-thermal catalytic process owing to their higher solar energy utilization efficiency as compared to other conventional photocatalysts. In the present review, the fundamental mechanism of the LSPR effect was displayed by plasmonic photocatalysts and its role in the performance of certain photo-thermal catalytic reaction was briefly explained. Under solar irradiation, photo-thermally induced heat and light properties of the plasmonic and non-plasmonic nanomaterials can be utilized to enhance catalytic conversions, either individually or in a synergistic manner. The exact interaction mechanism of both approaches during a photocatalytic reaction still needs to be further discovered; however, an insightful revision of the methodologies to differentiate the leading pathway was included. Several types of design and material selection techniques were compiled in order to enhance the light absorption range and photo-thermal transformation efficiency of the plasmonic catalysts, concluding that controlled size and tailored morphology containing nano-defective structures (rods, bars, wires, etc.) could significantly control the plasmonic ability and generate high-energy electrons. Moreover, hybrid heterostructures (metal–semiconductor, metal–porous, and core–shell hybrid systems), due to their dual nature, could effectively tune the photo, thermal, and electrochemical properties of the photo-catalysts. Furthermore, we also summarized newly developed plasmonic catalysts and their synergistic photo-thermal catalytic performances in various photocatalytic processes of energy production and environment remediation, including CO_2 reduction, H_2 production, organic pollutant degradation, and organic compound synthesis. The wide range of catalytic applications, along with the prospect of tailoring morphology, and tuning the electrical, thermal, and optical properties of photocatalysts, signifies the potential and sustainability of the photo-thermal catalytic regime.

Indeed, photo-thermal catalysis has a wide range of applications, but the large-scale implementation is still facing various challenges, as there are few studies on synergistic interaction mechanisms and competence with conventional thermal methods. Primarily, the heat and light contributions in photo-thermal catalysis must be distinguished and quantified. The synergistic interactions between photo and thermal catalysis are very diverse and complex, and the fundamental mechanism of synergy should be well distinct and estimated, which is crucial to synthetically enhance the synergy among photo and thermal catalysis, and to amplify the utilization of solar energy. To identify the relative contributions, a precise estimation of the local heating of the photocatalyst is required. In the view of this, the photo-thermal technique has major benefits as it has the potential to enhance selectivity to encounter targets by choosing appropriate light wavelengths. Hot-carrier chemistry has proven to be more proficient than the thermochemical route in triggering a particular reaction pathway by restrictively exciting molecular bonds of adsorbent. In comparison with traditional heat-based catalytic reactions, photo-thermal catalysis retains high production efficiency even under harsh conditions due to its solar energy utilization capability, which is not only beneficial in case of adaptability, but also in the vein of reusability and strength of catalysts.

As mentioned above, the size and shape of plasmonic catalysts have a strong impact on the hot charge generation and transfer process, which clearly signifies the importance of photochemical contributions during a photo-thermal catalytic reaction. Furthermore, only the high-energy charge carriers can pass the Schottky barrier at the metal–semiconductor heterojunction interface, so the efficiency of the charge transfer is not only dependent on the hot electron energy level, but also on the length of the Schottky barrier. Therefore, it can be an effective strategy to promote the charge transfer by tuning the energy bands of the semiconductors using doping or vacancy formation techniques. In addition, some other designing strategies, such as metal loading, high-adsorption-capacity intermediates, and small-size nanoparticles, also determine the hot electron transfer rate; hence, all these designing parameters should be prudently considered when constructing a photo-thermal nanomaterial. On the other hand, in thermocatalytic reactions, the nanomaterials with a

wide light absorbance range, lower heat loss, and less irradiative emissions have greater potential to increase the catalytic performance. Non-stoichiometric materials with more vacancies or defects are mainly preferred. In general, a perfect design and an appropriate engineering of the photocatalyst can develop an ideal synergy between photo and thermal contributions, thus resulting in excellent photo-thermal activity.

Nonetheless, photo-thermal catalysis has limitations, which hinder its broad application in the field of energy production and conversion, environmental remediation, and organic compound synthesis. Some of these are mentioned below.

1. Photo-thermal catalysis is far better than the other conventional technologies as it can perform efficiently under mild conditions, but the main challenge is to incorporate the light into photo-thermal systems; for that purpose, suitable photoreactors with higher solar energy harvesting and utilization efficiency are required. However, various reported studies indicated that the application of continuous flow systems is more feasible for large-scale implementation, instead of applying batch experimental systems. Thereby, more attention should be paid in this approach to develop highly efficient and configured reactors.
2. Among the extensive amount of investigations available on photo-thermal catalysis, few have explained the dominant reaction pathway that governs the actual reaction mechanism. Fundamentally, more research in this area is required.
3. Although several different plasmonic materials, other than the noble plasmonic metals, have been revealed in recent years, a lot still needs to be discovered. In recent years, chalcogenides and nitrides have been extensively applied in photo-thermal catalytic processes due to their efficient photo-thermal ability.
4. For instance, the CO_2 conversion process mainly yields CO and CH_4; however, more attention should be paid towards other valuable alkanes and alkenes (olefins), such as propylene, formic acid, ethylene, etc. In addition, one of the most vigorous characteristics in photo-thermal catalysis is the selectivity control, so more information on this could be favorable for designing high-selectivity photo-thermal catalytic systems.
5. The stability and recyclability of photocatalysts are also major challenges, as most stability assessment experiments are severely constrained to a few hours. Therefore, highly sustainable photocatalysts are urgently needed in order to meet these large-scale requirements.

Author Contributions: Initial draft and layout, A.S.; revision and proofread, A.A.D. and Y.L.; supervised and final validation, C.W. All authors have read and agreed to the published version of the manuscript.

Funding: This work was supported by the National Natural Science Foundation of China (Nos. 21976116, 52161145409), the Shaanxi Science and Technology Program (2020KWZ-005), and the SAFEA of China ("Belt and Road" Innovative Exchange Foreign Expert Project). We would also like to acknowledge all contributors for their efforts. The authors would like to acknowledge the China postdoctoral foundation for regional support research grant (2021M693857).

Data Availability Statement: Not applicable.

Acknowledgments: Not applicable.

Conflicts of Interest: The authors declare no conflict of interest.

References

1. Zhao, Y.; Gao, W.; Li, S.; Williams, G.R.; Mahadi, A.H.; Ma, D. Solar-versus Thermal-Driven Catalysis for Energy Conversion. *Joule* **2019**, *3*, 920–937. [CrossRef]
2. Jeong, G.H.; Sasikala, S.P.; Yun, T.; Lee, G.Y.; Lee, W.J.; Kim, S.O. Nanoscale Assembly of 2D Materials for Energy and Environmental Applications. *Adv. Mater.* **2020**, *32*, e1907006. [CrossRef] [PubMed]
3. Lim, H.; Kim, H.S.; Qazi, R.; Kwon, Y.; Jeong, J.; Yeo, W. Advanced Soft Materials, Sensor Integrations, and Applications of Wearable Flexible Hybrid Electronics in Healthcare, Energy, and Environment. *Adv. Mater.* **2019**, *32*, e1901924. [CrossRef] [PubMed]

4. Geng, D.; Yang, H.Y. Recent Advances in Growth of Novel 2D Materials: Beyond Graphene and Transition Metal Dichalcogenides. *Adv. Mater.* **2018**, *30*, e1800865. [CrossRef] [PubMed]
5. O'Regan, B.; Grätzel, M. A low-cost, high-efficiency solar cell based on dye-sensitized colloidal TiO_2 films. *Nature* **1991**, *353*, 737–740. [CrossRef]
6. Kong, Z.-C.; Liao, J.-F.; Dong, Y.-J.; Xu, Y.-F.; Chen, H.-Y.; Kuang, D.-B.; Su, C.-Y. Core@Shell $CsPbBr_3$@Zeolitic Imidazolate Framework Nanocomposite for Efficient Photocatalytic CO_2 Reduction. *ACS Energy Lett.* **2018**, *3*, 2656–2662. [CrossRef]
7. Manjavacas, A.; Liu, J.G.; Kulkarni, V.; Nordlander, P. Plasmon-Induced Hot Carriers in Metallic Nanoparticles. *ACS Nano* **2014**, *8*, 7630–7638. [CrossRef]
8. Petryayeva, E.; Krull, U.J. Localized surface plasmon resonance: Nanostructures, bioassays and biosensing—A review. *Anal. Chim. Acta* **2011**, *706*, 8–24. [CrossRef]
9. Richardson, H.H.; Hickman, Z.N.; Govorov, A.O.; Thomas, A.C.; Zhang, W.; Kordesch, M.E. Thermooptical Properties of Gold Nanoparticles Embedded in Ice: Characterization of Heat Generation and Melting. *Nano Lett.* **2006**, *6*, 783–788. [CrossRef]
10. Thermo-plasmonics: Using metallic nanostructures as nano-sources of heat. *Laser Photon-Rev.* **2019**, *7*, 170. [CrossRef]
11. Politano, A.; Argurio, P.; Di Profio, G.; Sanna, V.; Cupolillo, A.; Chakraborty, S.; Arafat, H.A.; Curcio, E. Photothermal Membrane Distillation for Seawater Desalination. *Adv. Mater.* **2017**, *29*, 1603504. [CrossRef] [PubMed]
12. Nguyen, N.T.; Xia, M.; Duchesne, P.N.; Wang, L.; Mao, C.; Jelle, A.A.; Yan, T.; Li, P.; Lu, Z.-H.; Ozin, G.A. Enhanced CO_2 Photocatalysis by Indium Oxide Hydroxide Supported on TiN@TiO_2 Nanotubes. *Nano Lett.* **2021**, *21*, 1311–1319. [CrossRef] [PubMed]
13. Zhu, L.; Gao, M.; Peh, C.K.N.; Ho, G.W. Solar-driven photothermal nanostructured materials designs and prerequisites for evaporation and catalysis applications. *Mater. Horiz.* **2018**, *5*, 323–343. [CrossRef]
14. Li, S.; Miao, P.; Zhang, Y.; Wu, J.; Zhang, B.; Du, Y.; Han, X.; Sun, J.; Xu, P. Recent Advances in Plasmonic Nanostructures for Enhanced Photocatalysis and Electrocatalysis. *Adv. Mater.* **2020**, *33*, e2000086. [CrossRef] [PubMed]
15. O'Brien, P.G.; Sandhel, A.; Wood, T.E.; Jelle, A.A.; Hoch, L.B.; Perovic, D.D.; Mims, C.A.; Ozin, G.A. Photomethanation of Gaseous CO_2over Ru/Silicon Nanowire Catalysts with Visible and Near-Infrared Photons. *Adv. Sci.* **2014**, *1*, 1400001. [CrossRef]
16. Jia, J.; O'Brien, P.G.; He, L.; Qiao, Q.; Fei, T.; Reyes, L.M.; Burrow, T.E.; Dong, Y.; Liao, K.; Varela, M.; et al. Visible and Near-Infrared Photothermal Catalyzed Hydrogenation of Gaseous CO_2 over Nanostructured Pd@Nb_2O_5. *Adv. Sci.* **2016**, *3*, 1600189. [CrossRef]
17. Zhang, R.; Xu, J.; Lu, C.; Xu, Z. Photothermal application of SmCoO3/SBA-15 catalysts synthesized by impregnation method. *Mater. Lett.* **2018**, *228*, 199–202. [CrossRef]
18. Vu, N.; Kaliaguine, S.; Do, T. Plasmonic Photocatalysts for Sunlight-Driven Reduction of CO_2: Details, Developments, and Perspectives. *ChemSusChem* **2020**, *13*, 3967–3991. [CrossRef]
19. Ma, X.; Dai, Y.; Yu, L.; Huang, B. Energy transfer in plasmonic photocatalytic composites. *Light Sci. Appl.* **2016**, *5*, e16017. [CrossRef]
20. Kumar, V.; O'Donnell, S.; Sang, D.L.; Maggard, P.A.; Wang, G. Harnessing Plasmon-Induced Hot Carriers at the Interfaces With Ferroelectrics. *Front. Chem.* **2019**, *7*, 299. [CrossRef]
21. Gellé, A.; Jin, T.; De La Garza, L.; Price, G.D.; Besteiro, L.V.; Moores, A. Applications of Plasmon-Enhanced Nanocatalysis to Organic Transformations. *Chem. Rev.* **2019**, *120*, 986–1041. [CrossRef] [PubMed]
22. Hou, W.B.; Cronin, S.B. A Review of Surface Plasmon Resonance-Enhanced Photocatalysis. *Adv. Funct. Mater.* **2012**, *23*, 1612–1619. [CrossRef]
23. Qian, K.; Sweeny, B.C.; Johnston-Peck, A.C.; Niu, W.; Graham, J.O.; DuChene, J.S.; Qiu, J.; Wang, Y.-C.; Engelhard, M.H.; Su, D.; et al. Surface Plasmon-Driven Water Reduction: Gold Nanoparticle Size Matters. *J. Am. Chem. Soc.* **2019**, *136*, 9842–9845. [CrossRef] [PubMed]
24. Kale, M.J.; Avanesian, T.; Christopher, P. Direct Photocatalysis by Plasmonic Nanostructures. *ACS Catal.* **2014**, *4*, 116–128. [CrossRef]
25. Christopher, P.; Xin, H.; Linic, S. Visible-light-enhanced catalytic oxidation reactions on plasmonic silver nanostructures. *Nat. Chem.* **2014**, *3*, 467–472. [CrossRef]
26. Zhang, Y.; He, S.; Guo, W.; Hu, Y.; Huang, J.; Mulcahy, J.R.; Wei, W.D. Surface-Plasmon-Driven Hot Electron Photochemistry. *Chem. Rev.* **2018**, *118*, 2927–2954. [CrossRef]
27. Hartland, G.V.; Besteiro, L.V.; Johns, P.; Govorov, A.O. What's so Hot about Electrons in Metal Nanoparticles? *ACS Energy Lett.* **2017**, *2*, 1641–1653. [CrossRef]
28. Christopher, P.; Moskovits, M. Hot Charge Carrier Transmission from Plasmonic Nanostructures. *Annu. Rev. Phys. Chem.* **2017**, *68*, 379–398. [CrossRef]
29. Boerigter, C.; Campana, R.; Morabito, M.; Linic, S. Evidence and implications of direct charge excitation as the dominant mechanism in plasmon-mediated photocatalysis. *Nat. Commun.* **2016**, *7*, 10545. [CrossRef]
30. Sarina, S.; Jaatinen, E.; Xiao, Q.; Huang, Y.M.; Christopher, P.; Zhao, J.C.; Zhu, H.Y. Photon Energy Threshold in Direct Photocatalysis with Metal Nanoparticles: Key Evidence from the Action Spectrum of the Reaction. *J. Phys. Chem. Lett.* **2017**, *8*, 2526–2534. [CrossRef]
31. Mukherjee, S.; Zhou, L.; Goodman, A.M.; Large, N.; Ayala-Orozco, C.; Zhang, Y.; Nordlander, P.; Halas, N.J. Hot-Electron-Induced Dissociation of H_2on Gold Nanoparticles Supported on SiO_2. *J. Am. Chem. Soc.* **2014**, *136*, 64–67. [CrossRef] [PubMed]

32. Marimuthu, A.; Zhang, J.; Linic, S. Tuning Selectivity in Propylene Epoxidation by Plasmon Mediated Photo-Switching of Cu Oxidation State. *Science* **2013**, *339*, 1590–1593. [CrossRef] [PubMed]
33. Mukherjee, S.; Libisch, F.; Large, N.; Neumann, O.; Brown, L.V.; Cheng, J.; Lassiter, J.B.; Carter, E.A.; Nordlander, P.; Halas, N.J. Hot Electrons Do the Impossible: Plasmon-Induced Dissociation of H_2 on Au. *Nano Lett.* **2012**, *13*, 240–247. [CrossRef] [PubMed]
34. Bauer, C.; Abid, J.-P.; Fermin, D.; Girault, H.H. Ultrafast chemical interface scattering as an additional decay channel for nascent nonthermal electrons in small metal nanoparticles. *J. Chem. Phys.* **2004**, *120*, 9302–9315. [CrossRef] [PubMed]
35. Boerigter, C.; Aslam, U.; Linic, S. Mechanism of Charge Transfer from Plasmonic Nanostructures to Chemically Attached Materials. *ACS Nano* **2016**, *10*, 6108–6115. [CrossRef]
36. Foerster, B.; Joplin, A.; Kaefer, K.; Celiksoy, S.; Link, S.; Sönnichsen, C. Chemical Interface Damping Depends on Electrons Reaching the Surface. *ACS Nano* **2017**, *11*, 2886–2893. [CrossRef]
37. Wang, M.; Ye, M.; Iocozzia, J.; Lin, C.; Lin, Z. Plasmon-Mediated Solar Energy Conversion via Photocatalysis in Noble Metal/Semiconductor Composites. *Adv. Sci.* **2016**, *3*, 1600024. [CrossRef]
38. Baldoví, H.G.; Neaţu, S.; Khan, A.; Asiri, A.M.; Kosa, S.A.; Garcia, H. Understanding the Origin of the Photocatalytic CO_2 Reduction by Au- and Cu-Loaded TiO_2: A Microsecond Transient Absorption Spectroscopy Study. *J. Phys. Chem. C* **2015**, *119*, 6819–6827. [CrossRef]
39. DuChene, J.S.; Sweeny, B.C.; Johnston-Peck, A.C.; Su, D.; Stach, E.A.; Wei, W.D. Prolonged Hot Electron Dynamics in Plasmonic-Metal/Semiconductor Heterostructures with Implications for Solar Photocatalysis. *Angew. Chem. Int. Ed.* **2014**, *53*, 7887–7891. [CrossRef]
40. Khan, M.R.; Chuan, T.W.; Yousuf, A.; Chowdhury, M.N.K.; Cheng, C.K. Schottky barrier and surface plasmonic resonance phenomena towards the photocatalytic reaction: Study of their mechanisms to enhance photocatalytic activity. *Catal. Sci. Technol.* **2015**, *5*, 2522–2531. [CrossRef]
41. Marchuk, K.; Willets, K.A. Localized surface plasmons and hot electrons. *Chem. Phys.* **2014**, *445*, 95–104. [CrossRef]
42. Schuck, P.J. Hot electrons go through the barrier. *Nat. Nanotechnol.* **2014**, *8*, 799–800. [CrossRef]
43. Furube, A.; Du, L.; Hara, K.; Katoh, R.; Tachiya, M. Ultrafast Plasmon-Induced Electron Transfer from Gold Nanodots into TiO2 Nanoparticles. *J. Am. Chem. Soc.* **2007**, *129*, 14852–14853. [CrossRef] [PubMed]
44. White, T.P.; Catchpole, K.R. Plasmon-enhanced internal photoemission for photovoltaics: Theoretical efficiency limits. *Appl. Phys. Lett.* **2012**, *101*, 073905. [CrossRef]
45. Tan, S.; Argondizzo, A.; Ren, J.; Liu, L.; Zhao, J.; Petek, H. Plasmonic coupling at a metal/semiconductor interface. *Nat. Photonics* **2017**, *11*, 806–812. [CrossRef]
46. Yu, Y.; Ji, Z.; Zu, S.; Du, B.; Kang, Y.; Li, Z.; Zhou, Z.; Shi, K.; Fang, Z. Ultrafast Plasmonic Hot Electron Transfer in Au Nanoantenna/MoS_2Heterostructures. *Adv. Funct. Mater.* **2016**, *26*, 6394–6401. [CrossRef]
47. Mateo, D.; Cerrillo, J.L.; Durini, S.; Gascon, J. Fundamentals and applications of photo-thermal catalysis. *Chem. Soc. Rev.* **2020**, *50*, 2173–2210. [CrossRef]
48. Ghoussoub, M.; Xia, M.; Duchesne, P.N.; Segal, D.; Ozin, G. Principles of photothermal gas-phase heterogeneous CO_2 catalysis. *Energy Environ. Sci.* **2019**, *12*, 1122–1142. [CrossRef]
49. Li, Q.; Zhang, Z.; Haque, S.S.; Zhang, M.; Xia, L. Localized surface plasmon resonance effects by naturally occurring Chinese yam particles. *J. Appl. Phys.* **2010**, *108*, 123502. [CrossRef]
50. Forno, S.D.; Ranno, L.; Lischner, J. Material, Size, and Environment Dependence of Plasmon-Induced Hot Carriers in Metallic Nanoparticles. *J. Phys. Chem. C* **2018**, *122*, 8517–8527. [CrossRef]
51. Rycenga, M.; Cobley, C.M.; Zeng, J.; Li, W.; Moran, C.H.; Zhang, Q.; Qin, D.; Xia, Y. Controlling the Synthesis and Assembly of Silver Nanostructures for Plasmonic Applications. *Chem. Rev.* **2011**, *111*, 3669–3712. [CrossRef]
52. Zhang, Q.; Li, W.; Moran, C.; Zeng, J.; Chen, J.; Wen, L.-P.; Xia, Y. Seed-Mediated Synthesis of Ag Nanocubes with Controllable Edge Lengths in the Range of 30−200 nm and Comparison of Their Optical Properties. *J. Am. Chem. Soc.* **2010**, *132*, 11372–11378. [CrossRef] [PubMed]
53. Mulvihill, M.J.; Ling, X.Y.; Henzie, J.; Yang, P. Anisotropic Etching of Silver Nanoparticles for Plasmonic Structures Capable of Single-Particle SERS. *J. Am. Chem. Soc.* **2010**, *132*, 268–274. [CrossRef]
54. Zhang, H.; Govorov, A.O. Optical Generation of Hot Plasmonic Carriers in Metal Nanocrystals: The Effects of Shape and Field Enhancement. *J. Phys. Chem. C* **2014**, *118*, 7606–7614. [CrossRef]
55. Besteiro, L.V.; Govorov, A.O. Amplified Generation of Hot Electrons and Quantum Surface Effects in Nanoparticle Dimers with Plasmonic Hot Spots. *J. Phys. Chem. C* **2016**, *120*, 19329–19339. [CrossRef]
56. Lim, J.; Hippalgaonkar, K.; Andrews, S.C.; Majumdar, A.; Yang, P. Quantifying Surface Roughness Effects on Phonon Transport in Silicon Nanowires. *Nano Lett.* **2012**, *12*, 2475–2482. [CrossRef] [PubMed]
57. Fang, Z.; Jiao, S.; Kang, Y.; Pang, G.; Feng, S. Photothermal Conversion of W18 O49 with a Tunable Oxidation State. *ChemistryOpen* **2017**, *6*, 261–265. [CrossRef] [PubMed]
58. Wang, L.; Dong, Y.; Yan, T.; Hu, Z.; Jelle, A.A.; Meira, D.M.; Duchesne, P.N.; Loh, J.Y.Y.; Qiu, C.; Storey, E.E.; et al. Black indium oxide a photothermal CO_2 hydrogenation catalyst. *Nat. Commun.* **2020**, *11*, 2432. [CrossRef]
59. Zhang, X.; Ke, X.; Zhu, H. Zeolite-Supported Gold Nanoparticles for Selective Photooxidation of Aromatic Alcohols under Visible-Light Irradiation. *Chem.–A Eur. J.* **2012**, *18*, 8048–8056. [CrossRef]

60. Das, S.; Pérez-Ramírez, J.; Gong, J.; Dewangan, N.; Hidajat, K.; Gates, B.C.; Kawi, S. Core–shell structured catalysts for thermocatalytic, photocatalytic, and electrocatalytic conversion of CO_2. *Chem. Soc. Rev.* **2020**, *49*, 2937–3004. [CrossRef]
61. Guo, L.; Sun, Q.; Marcus, K.; Hao, Y.; Deng, J.; Bi, K.; Yang, Y. Photocatalytic glycerol oxidation on Au_xCu–CuS@TiO_2 plasmonic heterostructures. *J. Mater. Chem. A* **2018**, *6*, 22005–22012. [CrossRef]
62. Huang, H.; Zhang, L.; Lv, Z.; Long, R.; Zhang, C.; Lin, Y.; Wei, K.; Wang, C.; Chen, L.; Li, Z.-Y.; et al. Unraveling Surface Plasmon Decay in Core–Shell Nanostructures toward Broadband Light-Driven Catalytic Organic Synthesis. *J. Am. Chem. Soc.* **2016**, *138*, 6822–6828. [CrossRef]
63. Wang, F.; Li, C.; Chen, H.; Jiang, R.; Sun, L.-D.; Li, Q.; Wang, J.; Yu, J.C.; Yan, C.-H. Plasmonic Harvesting of Light Energy for Suzuki Coupling Reactions. *J. Am. Chem. Soc.* **2013**, *135*, 5588–5601. [CrossRef]
64. Manthiram, K.; Alivisatos, A.P. Tunable Localized Surface Plasmon Resonances in Tungsten Oxide Nanocrystals. *J. Am. Chem. Soc.* **2012**, *134*, 3995–3998. [CrossRef] [PubMed]
65. Gu, Y.; Jiao, Y.; Zhou, X.; Wu, A.; Buhe, B.; Fu, H. Strongly coupled Ag/TiO2 heterojunctions for effective and stable photothermal catalytic reduction of 4-nitrophenol. *Nano Res.* **2017**, *11*, 126–141. [CrossRef]
66. Lai, B.-H.; Lin, Y.-R.; Chen, D.-H. Fabrication of LaB6@SiO2/Au composite nanoparticles as a catalyst with near infrared photothermally enhanced activity. *Chem. Eng. J.* **2013**, *223*, 418–424. [CrossRef]
67. Wang, C.; Ranasingha, O.; Natesakhawat, S.; Ohodnicki, P.R.; Andio, M.; Lewis, J.P.; Matranga, C. Visible light plasmonic heating of Au–ZnO for the catalytic reduction of CO_2. *Nanoscale* **2013**, *5*, 6968–6974. [CrossRef]
68. Zou, J.; Si, Z.; Cao, Y.; Ran, R.; Wu, X.; Weng, D. Localized Surface Plasmon Resonance Assisted Photothermal Catalysis of CO and Toluene Oxidation over Pd–CeO_2 Catalyst under Visible Light Irradiation. *J. Phys. Chem. C* **2016**, *120*, 29116–29125. [CrossRef]
69. Ren, J.; Ouyang, S.; Xu, H.; Meng, X.; Wang, T.; Wang, D.; Ye, J. Targeting Activation of CO_2 and H_2over Ru-Loaded Ultrathin Layered Double Hydroxides to Achieve Efficient Photothermal CO_2 Methanation in Flow-Type System. *Adv. Energy Mater.* **2016**, *7*, 1601657. [CrossRef]
70. Zhang, H.; Wang, T.; Wang, J.; Liu, H.; Dao, T.D.; Li, M.; Liu, G.; Meng, X.; Chang, K.; Shi, L.; et al. Surface-Plasmon-Enhanced Photodriven CO_2 Reduction Catalyzed by Metal–Organic-Framework-Derived Iron Nanoparticles Encapsulated by Ultrathin Carbon Layers. *Adv. Mater.* **2016**, *28*, 3703–3710. [CrossRef]
71. Robatjazi, H.; Zhao, H.; Swearer, D.F.; Hogan, N.J.; Zhou, L.; Alabastri, A.; McClain, M.J.; Nordlander, P.; Halas, N.J. Plasmon-induced selective carbon dioxide conversion on earth-abundant aluminum-cuprous oxide antenna-reactor nanoparticles. *Nat. Commun.* **2017**, *8*, 27. [CrossRef] [PubMed]
72. Wang, J.; Sun, X. Olivine $LiFePO_4$: The remaining challenges for future energy storage. *Energy Environ. Sci.* **2015**, *8*, 1110–1138. [CrossRef]
73. Wang, X.; He, Y.; Hu, Y.; Jin, G.; Jiang, B.; Huang, Y. Photothermal-conversion-enhanced photocatalytic activity of flower-like CuS superparticles under solar light irradiation. *Sol. Energy* **2018**, *170*, 586–593. [CrossRef]
74. Yang, Q.; Xu, Q.; Yu, S.; Jiang, H.-L. Pd Nanocubes@ZIF-8: Integration of Plasmon-Driven Photothermal Conversion with a Metal-Organic Framework for Efficient and Selective Catalysis. *Angew. Chem. Int. Ed.* **2016**, *55*, 3685–3689. [CrossRef] [PubMed]
75. Yang, Y.; Li, Y.; Zeng, M.; Mao, M.; Lan, L.; Liu, H.; Chen, J.; Zhao, X. UV–vis-infrared light-driven photothermocatalytic abatement of CO on Cu doped ramsdellite MnO_2 nanosheets enhanced by a photoactivation effect. *Appl. Catal. B Environ.* **2017**, *224*, 751–760. [CrossRef]
76. Zheng, Y.; Wang, W.; Jiang, D.; Zhang, L.; Li, X.; Wang, Z. Ultrathin mesoporous Co_3O_4 nanosheets with excellent photo-/thermo-catalytic activity. *J. Mater. Chem. A* **2015**, *4*, 105–112. [CrossRef]
77. Tu, W.; Zhou, Y.; Li, H.; Li, P.; Zou, Z. Au@TiO_2yolk–shell hollow spheres for plasmon-induced photocatalytic reduction of CO_2 to solar fuel via a local electromagnetic field. *Nanoscale* **2015**, *7*, 14232–14236. [CrossRef]
78. Feng, S.; Wang, M.; Zhou, Y.; Li, P.; Tu, W.; Zou, Z. Double-shelled plasmonic Ag-TiO_2 hollow spheres toward visible light-active photocatalytic conversion of CO_2 into solar fuel. *APL Mater.* **2015**, *3*, 104416. [CrossRef]
79. Do, J.Y.; Chava, R.K.; Mandari, K.K.; Park, N.-K.; Ryu, H.-J.; Seo, M.W.; Lee, D.; Senthil, T.; Kang, M. Selective methane production from visible-light-driven photocatalytic carbon dioxide reduction using the surface plasmon resonance effect of superfine silver nanoparticles anchored on lithium titanium dioxide nanocubes (Ag@LixTiO2). *Appl. Catal. B Environ.* **2018**, *237*, 895–910. [CrossRef]
80. Xu, F.; Meng, K.; Cheng, B.; Yu, J.; Ho, W. Enhanced Photocatalytic Activity and Selectivity for CO $_2$ Reduction over a TiO_2 Nanofibre Mat Using Ag and MgO as Bi-Cocatalyst. *ChemCatChem* **2019**, *11*, 465–472. [CrossRef]
81. Neaţu, Ş.; Maciá-Agulló, J.A.; Concepción, P.; Garcia, H. Gold–Copper Nanoalloys Supported on TiO_2 as Photocatalysts for CO_2 Reduction by Water. *J. Am. Chem. Soc.* **2014**, *136*, 15969–15976. [CrossRef] [PubMed]
82. Zhao, J.; Liu, B.; Meng, L.; He, S.; Yuan, R.; Hou, Y.; Ding, Z.; Lin, H.; Zhang, Z.; Wang, X.; et al. Plasmonic control of solar-driven CO_2 conversion at the metal/ZnO interfaces. *Appl. Catal. B Environ.* **2019**, *256*, 117823. [CrossRef]
83. Xin, Z.; Lu, L.; Wang, B.; Wang, X.; Zhu, K.; Xu, Z.; Yu, Z.; Yan, S.; Zou, Z. Lewis acid activated CO_2 reduction over a Ni modified Ni–Ge hydroxide driven by visible-infrared light. *Dalton Trans.* **2018**, *48*, 1672–1679. [CrossRef]
84. Shen, J.; Chen, Z.; Han, S.; Zhang, H.; Xu, H.; Xu, C.; Ding, Z.; Yuan, R.; Chen, J.; Long, J. Plasmonic Electrons-Driven Solar-to-Hydrocarbon Conversion over Au NR@ZnO Core-Shell Nanostructures. *ChemCatChem* **2020**, *12*, 2989–2994. [CrossRef]
85. Yamazaki, Y.; Takeda, H.; Ishitani, O. Photocatalytic reduction of CO2 using metal complexes. *J. Photochem. Photobiol. C Photochem. Rev.* **2015**, *25*, 106–137. [CrossRef]

86. Chen, Y.-Z.; Wang, Z.U.; Wang, H.; Lu, J.; Yu, S.-H.; Jiang, H.-L. Singlet Oxygen-Engaged Selective Photo-Oxidation over Pt Nanocrystals/Porphyrinic MOF: The Roles of Photothermal Effect and Pt Electronic State. *J. Am. Chem. Soc.* **2017**, *139*, 2035–2044. [CrossRef]
87. Kumar, D.; Park, C.H.; Kim, C.S. Robust Multimetallic Plasmonic Core–Satellite Nanodendrites: Highly Effective Visible-Light-Induced Colloidal CO_2 Photoconversion System. *ACS Sustain. Chem. Eng.* **2018**, *6*, 8604–8614. [CrossRef]
88. Meng, X.; Wang, T.; Liu, L.; Ouyang, S.; Li, P.; Hu, H.; Kako, T.; Iwai, H.; Tanaka, A.; Ye, J. Photothermal Conversion of CO_2 into CH_4 with H_2 over Group VIII Nanocatalysts: An Alternative Approach for Solar Fuel Production. *Angew. Chem.* **2014**, *126*, 11662–11666. [CrossRef]
89. Chen, G.; Gao, R.; Zhao, Y.; Li, Z.; Waterhouse, G.I.N.; Shi, R.; Zhao, J.; Zhang, M.; Shang, L.; Sheng, G.; et al. Alumina-Supported CoFe Alloy Catalysts Derived from Layered-Double-Hydroxide Nanosheets for Efficient Photothermal CO_2 Hydrogenation to Hydrocarbons. *Adv. Mater.* **2017**, *30*, 1704663. [CrossRef]
90. Wang, L.; Wang, Y.; Cheng, Y.; Liu, Z.; Guo, Q.; Ha, M.N.; Zhao, Z. Hydrogen-treated mesoporous WO_3 as a reducing agent of CO_2 to fuels (CH_4 and CH_3OH) with enhanced photothermal catalytic performance. *J. Mater. Chem. A* **2016**, *4*, 5314–5322. [CrossRef]
91. Ha, M.N.; Lu, G.; Liu, Z.; Wang, L.; Zhao, Z. 3DOM-$LaSrCoFeO_{6-\delta}$ as a highly active catalyst for the thermal and photothermal reduction of CO_2 with H_2O to CH_4. *J. Mater. Chem. A* **2016**, *4*, 13155–13165. [CrossRef]
92. Ma, R.; Sun, J.; Li, D.H.; Wei, J.J. Review of synergistic photo-thermo-catalysis: Mechanisms, materials and applications. *Int. J. Hydrog. Energy* **2020**, *45*, 30288–30324. [CrossRef]
93. Peh, C.K.N.; Gao, M.; Ho, G.W. Harvesting broadband absorption of the solar spectrum for enhanced photocatalytic H_2 generation. *J. Mater. Chem. A* **2015**, *3*, 19360–19367. [CrossRef]
94. Gao, M.; Connor, P.K.N.; Ho, G.W. Plasmonic photothermic directed broadband sunlight harnessing for seawater catalysis and desalination. *Energy Environ. Sci.* **2016**, *9*, 3151–3160. [CrossRef]
95. Liu, X.; Ye, L.; Ma, Z.; Han, C.; Wang, L.; Jia, Z.; Su, F.; Xie, H. Photothermal effect of infrared light to enhance solar catalytic hydrogen generation. *Catal. Commun.* **2017**, *102*, 13–16. [CrossRef]
96. Caudillo-Flores, U.; Agostini, G.; Marini, C.; Kubacka, A.; Fernández-García, M. Hydrogen thermo-photo production using Ru/TiO2: Heat and light synergistic effects. *Appl. Catal. B Environ.* **2019**, *256*, 117790. [CrossRef]
97. Gu, L.; Zhang, C.; Guo, Y.; Gao, J.; Yu, Y.; Zhang, B. Enhancing Electrocatalytic Water Splitting Activities via Photothermal Effect over Bifunctional Nickel/Reduced Graphene Oxide Nanosheets. *ACS Sustain. Chem. Eng.* **2019**, *7*, 3710–3714. [CrossRef]
98. Li, Y.; Huang, J.; Peng, T.; Xu, J.; Zhao, X. Photothermocatalytic Synergetic Effect Leads to High Efficient Detoxification of Benzene on TiO2 and Pt/TiO2 Nanocomposite. *ChemCatChem* **2010**, *2*, 1082–1087. [CrossRef]
99. Xie, W.; Li, Y.; Shi, W.; Zhao, L.; Zhao, X.; Fang, P.; Zheng, F.; Wang, S. Novel effect of significant enhancement of gas-phase photocatalytic efficiency for nano ZnO. *Chem. Eng. J.* **2012**, *213*, 218–224. [CrossRef]
100. Kim, J.-H.; Twaddle, K.M.; Hu, J.; Byun, H. Sunlight-Induced Synthesis of Various Gold Nanoparticles and Their Heterogeneous Catalytic Properties on a Paper-Based Substrate. *ACS Appl. Mater. Interfaces* **2014**, *6*, 11514–11522. [CrossRef]
101. Wang, G.; Huang, B.; Lou, Z.; Wang, Z.; Qin, X.; Zhang, X.; Dai, Y. Valence state heterojunction $Mn_3O_4/MnCO_3$: Photo and thermal synergistic catalyst. *Appl. Catal. B Environ.* **2015**, *180*, 6–12. [CrossRef]
102. Huang, Y.; Lu, Y.; Lin, Y.; Mao, Y.; Ouyang, G.; Liu, H.; Zhang, S.; Tong, Y. Cerium-based hybrid nanorods for synergetic photo-thermocatalytic degradation of organic pollutants. *J. Mater. Chem. A* **2018**, *6*, 24740–24747. [CrossRef]
103. Wang, F.; Huang, Y.; Chai, Z.; Zeng, M.; Li, Q.; Wang, Y.; Xu, D. Photothermal-enhanced catalysis in core–shell plasmonic hierarchical Cu_7S_4microsphere@zeolitic imidazole framework-8. *Chem. Sci.* **2016**, *7*, 6887–6893. [CrossRef] [PubMed]